Near-edge x-ray-absorption fine structure of crystalline silicon dioxides

Isao Tanaka, Jun Kawai, and Hirohiko Adachi
Department of Materials Science and Engineering, Kyoto University, Sakyo, Kyoto 606-01, Japan
(Received 5 October 1994; revised manuscript received 13 March 1995)

We present the results of first-principles molecular-orbital calculations of three forms of silicon dioxides, i.e., α-quartz, α-cristobalite, and β-cristobalite. The discrete variational (DV)-$X\alpha$ method is employed on model clusters of $(Si_5O_{16})^{12-}$ using minimal basis set. The Si-K, L_{23}, and O-K x-ray emission spectra (XES) and near-edge x-ray-absorption fine structures (NEXAFS) are compared with the calculated partial density of states (PDOS) following the electric dipole selection rule. We find that our PDOS at the ground state agrees well with fine structures of the experimental NEXAFS in the range of ≤ 30 eV as well as the XES. It means that the emission effects associated with the electronic transitions do not change the spectral shapes remarkably from those of the PDOS in these compounds. Assignments of all subband features are, therefore, successfuly made without taking these effects into account explicitly. Conduction band ≤ 30 eV from the edge can be decomposed into 12 subbands that are generated by bonding, antibonding, and nonbonding interactions of a_1, e, and two kinds of t_2 molecular orbitals in the individual $(SiO_4)^{4-}$ tetrahedron under T_d symmetry. The difference in the manner of $(SiO_4)^{4-}$ tetrahedral linkage among SiO_2 polymorphs is shown most clearly in the Si-L_{23} NEXAFS.

I. INTRODUCTION

Silicon dioxide (silica, SiO_2) is one of the most common materials on the Earth, and its valence-band structure has been studied extensively both from experiments and theories. Crystalline SiO_2 shows various polymorphs, all of which are formed by cornersharing of $(SiO_4)^{4-}$ tetrahedra except for a high-pressure form, stishovite. It is also very stable in a glassy form. The Si-O bond length in crystalline 4:2 coordinated SiO_2 varies in a relatively narrow range around 1.6 Å, but the Si-O-Si angle that defines the orientation of the tetrahedra relative to one another changes from 137 to 180°.

Photoelectron spectra [x-ray (XPS) or ultraviolet (UPS)] and x-ray emission spectra (XES) provide detailed information on the valence-band structure. XPS (UPS) and XES measurements on crystalline and glassy SiO_2 have been reported by many researchers.[1–5] In parallel to these experimental works, a number of electronic structure calculations of SiO_2 have been made to understand the valence-band structure as well as its nature of chemical bonding.[6–13] As already pointed out in the literature,[3,6,14] major features of the XPS of SiO_2 can be reproduced by the electronic calculation of a $(SiO_4)^{4-}$ tetrahedron in T_d symmetry.

The influence of the manner of $(SiO_4)^{4-}$ coupling on the valence-band structure was first experimentally examined by Wiech and Kurmaev[5] using Si K and L_{23} XES. Calculations of Si x-ray emission spectra of SiO_2 were reported by Cherlov *et al.*[11] and by Simunek, Vackar, and Wiech.[12] Though Cherlov *et al.*[11] failed to find good agreement between theoretical and experimental spectra, Simunek, Vackar, and Wiech,[12] who made calculations for α-quartz, have well reproduced the experimental spectra. Only a few experimental works on the conduction-band structure of SiO_2 have been reported because of experimental difficulties in the soft x-ray region. The Si L_{23} near-edge x-ray-absorption fine structure [NEXAFS or XANES (x-ray-absorption near-edge structure)] of glassy SiO_2 was first reported by Brown, Bachrach, and Skibowski.[15] More reliable data for glassy SiO_2 were recently reported.[16–18] High-resolution Si K and L_{23} NEXAFS of α-quartz were reported by Li *et al.*[19] O K-edge NEXAFS measurements were reported by Marcelli *et al.*,[20] and Lagarde *et al.*[21] Theoretical calculation of SiO_2 NEXAFS has not yet successfully reproduced the experimental spectra. It is true that Fujikawa[22] developed a short-range order multiple scattering theory and tried to simulate the L_{23}-edge NEXAFS of glassy SiO_2. Marchelli *et al.*[20] reported a multiple scattering calculation of SiO_2 O K-edge NEXAFS. Detailed structures of NEXAFS were, however, not well reproduced in these calculations. Sutherland *et al.*[23] employed a multiple-scattering $X\alpha$ (MS-$X\alpha$) calculation of NEXAFS for gas-phase $Si(CH_3)_x(OCH_3)_{4-x}$ in which they found analogy with that of solid SiO_2. Although the MS type calculations have been successful in many systems, they calculate the multiple-scattering phenomena by imposing a muffin-tin potential on the structure in question, and the results were thus dependent on the choice of the muffin-tin potential.[24] In addition to this disadvantage, use of a large number of scattering waves in the MS calculation lose simple but clear understanding of spectral features.

Recently, we have demonstrated that the near-edge structure of electron energy-loss spectra (ELNES) of MgO, which measures a similar transition to the NEXAFS, can be quantitatively well reproduced using a discrete-variational (DV) $X\alpha$ calculation on a model cluster.[25] Absolute transition energy, as well as fine structures of the ELNES in the range of ≤ 30 eV showed good agreement with partial density of states (PDOS) curves

0163-1829/95/52(16)/11733(7)/$06.00

we have obtained using minimal basis sets without inclusion of any adjustable parameters.

In this paper, we report the result of the DV-$X\alpha$ calculation on model clusters of three polymorphic forms of crystalline SiO_2. Although the DV-$X\alpha$ calculation of SiO_2 has recently been reported,[26,27] we pay special attention on the conduction-band structure and the influence of the linkage of $(SiO_4)^{4-}$ tetrahedra on the electronic structure in this work.

II. DISCRETE VARIATIONAL $X\alpha$ CLUSTER CALCULATION

First-principles molecular-orbital (MO) calculations were done by the Hartree-Fock-Slater method using the DV-$X\alpha$ computation code.[28] In this method, the exchange and correlation energies were taken into account by the use of the $X\alpha$ potential given by

$$V_{xc\uparrow}(r) = -3\alpha[(3/8\pi)\rho\uparrow(r)]^{1/3} , \quad (1)$$

where $\rho\uparrow(r)$ is the local charge density. The parameter α was fixed at 0.7. MO's were constructed by linear combination of atomic orbitals (LCAO), which were numerically generated. Basis functions of Si and O were $1s-3d$ and $1s-2p$ atomic orbitals (AO), respectively. A flat bottom and $1/r$ declining well potential defined in Eq. (2) was added only for the basis generation.

$$V(r) = V_0 \quad (r < R_0) ,$$
$$V(r) = V_0 R_0 / r \quad (r \geq R_0) . \quad (2)$$

In the present work, V_0 and R_0 were taken to be -49.0 eV (-3.6 Ry) and 1.43 Å (2.7 a.u.), respectively, for both Si and O AO's. As can be found in the Appendix, the electronic structure was found to be not significantly dependent on these values when they were chosen from the appropriate range.

Self-consistent charge calculation with the degree of convergence within 0.1% of the Mulliken charge was made to accomplish the self-consistent-field calculation practically.[29] An absolute value of the electronic transition was calculated using the "transition state" method proposed by Slater.[30] In this method, the transition energy can be calculated simply from the one-electron orbital energies obtained for the transition states in which half an electron was removed from the initial state to fill the final state. The total-energy difference between initial and final states was not necessarily calculated.

Calculation was made for three types of $(Si_5O_{16})^{12-}$ clusters consisting of 5 tetrahedral units taken from the crystalline data[31] of α-quartz (low-temperature form), α-cristobalite (low-temperature form) and β-cristobalite (high-temperature form). α-quartz has a hexagonal unit cell with lattice parameters of $a = 4.913$ Å and $c = 5.405$ Å. α-cristobalite has a tetragonal unit cell with $a = 4.973$ Å and $c = 6.926$ Å, and β-cristobalite has a cubic unit cell with $a = 7.16$ Å. These clusters were terminated only by oxygen atoms. In order to include the effect of Madelung potential outside the cluster in a simple manner, point charges with unit charge e were placed at all Si lattice sites that surround the cluster. The number of point charges was 12. Compared with the result without the inclusion of the point charges, MO levels originated from atoms located in the "skin" region of the clusters became closer to those from atoms at the "core" region. However, PDOS for Si and O atoms in the "core" region of the clusters were found to be almost independent of the magnitude of the point charges.

III. VALENCE-BAND SPECTRA

Figure 1 shows the calculated density of states (DOS) for three polymorphs in comparison with experimental x-ray photoemission spectra of α-quartz.[3] DOS was obtained simply by broadening of each MO levels with a Lorentzian function with a FWHM of 1.0 eV. The difference in intensity ratio of $2s$ and $2p$ bands between XPS data and calculated DOS is due to the difference in photoemission cross section of $2s$ and $2p$ AO's for high-energy x-ray excitation. Under Al $K\alpha_{12}$ radiation, ($h\nu = 1486.6$ eV), atomic photoionization cross sections

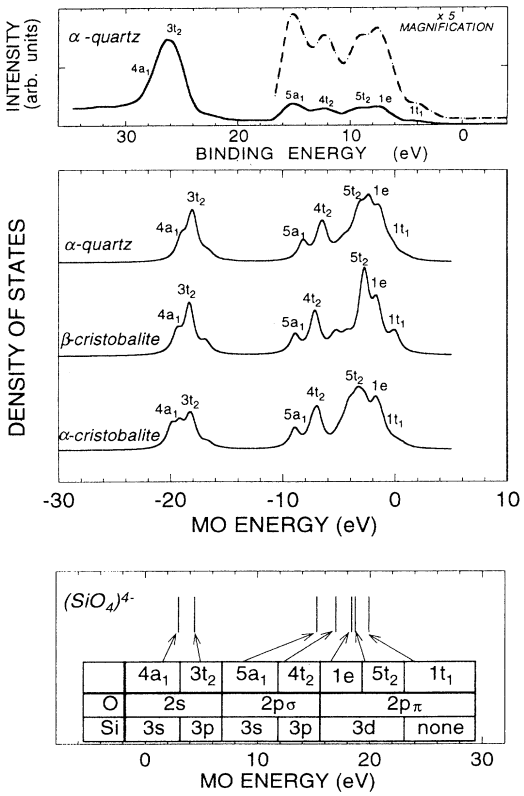

FIG. 1. Calculated valence-band DOS for three SiO_2 (middle) in comparison with experimental XPS of α-quartz taken from Ref. 3 (top) and MO levels of $(SiO_4)^{4-}$ together with their major components (bottom).

were reported to be 1.9×10^3 b for O $2s$ and 2.4×10^2 b for O $2p$ orbitals.[32] It means $2p$ PDOS is underestimated by a factor of 7.9 in the calculated spectra in order to compare with the experimental XPS.

Level schemes obtained from the calculation on $(SiO_4)^{4-}$ cluster in T_d symmetry and dominant AO components of each MO are also shown in Fig. 1. In the case of $(SiO_4)^{4-}$ cluster calculation, the Madelung potential was not considered. However, major features of the XPS of SiO_2 is reproduced by the calculation of the simple tetrahedron $(SiO_4)^{4-}$. Peaks in the experimental spectrum can be assigned using orbital notations under T_d symmetry in the same way as already made by Stephenson and Binkowski[3] who measured the XPS spectrum. However, the calculation only using a tetrahedron is obviously too simple, and different SiO_2 polymorphs cannot be discriminated through it.

Inclusion of a larger number of atoms for the cluster calculation makes it possible to calculate non-nearest-neighbor interaction of AO's. Thereby more detailed valence-band structure including the intensity ratios can be simulated. The intensity of $1t_1$ line is much weaker than the other O-$2p\pi$-originated lines, i.e., $1e$ and $5t_2$ in the experimental spectrum. This fact is well reproduced by the calculation of the larger clusters, and it can be ascribed to the non-nearest-neighbor interaction, which brings about the lowering of the energy of nonbonding MO's under the T_d symmetry. The reason for higher intensity of the O-$2p\sigma$-originated band ($5a_1$ and $4t_2$) compared with the O-$2p\pi$-originated band ($1e$ and $5t_2$) is explained by the difference in the photoemission cross sections of Si $3s$ from Si $3p$ and $3d$. For an excitation energy of 1486.6 eV, the cross section is greater by a factor of 5.9 for Si $3s$ than that of $3p$.[32] Although the cross section is not available for the Si $3d$ orbital, it can be assumed to be as small as that of Si $3p$. As shown in Fig. 2, the calculated intensity ratio between the O-$2p\sigma$-originated band and the O-$2p\pi$-originated band is in good agreement with the experimental O $K\alpha$ x-ray emission spectrum: It confirms the validity of the present calculation. DOS spectral shapes of SiO_2 polymorphs having different tetrahedral linkage are found to be similar to each other. The difference may be difficult to detect through the XPS experiment.

Since the upper valence band of SiO_2 mainly consists of O $2p$ AO's, and the selection rule for the O $K\alpha$ x-ray emission allows the transition from O $2p$ to O $1s$, the

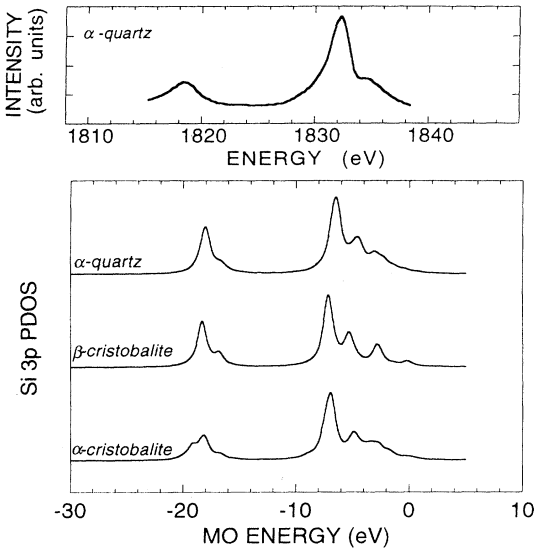

FIG. 3. Calculated Si $3p$ PDOS for three SiO_2 (bottom) in comparison with experimental Si K x-ray emission spectrum of α-quartz taken from Ref. 5 (top).

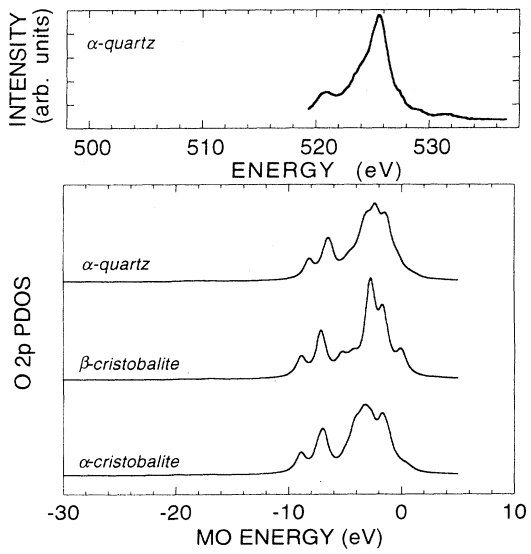

FIG. 2. Calculated O $2p$ PDOS for three SiO_2 (bottom) in comparison with experimental O K x-ray emission spectrum of α-quartz taken from Ref. 33 (top).

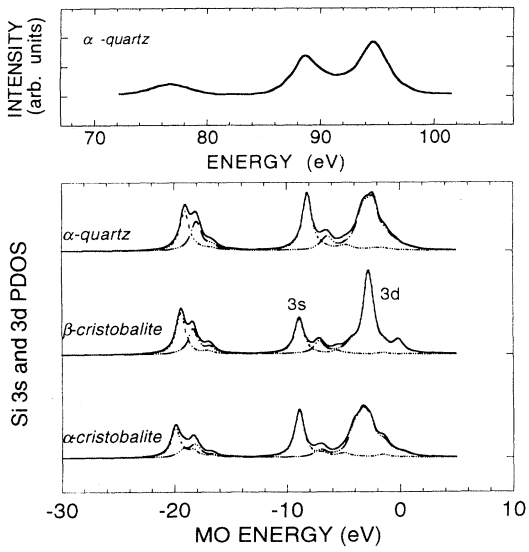

FIG. 4. Calculated Si $3s$ and $3d$ PDOS for three SiO_2 (bottom) in comparison with experimental Si L_{23} x-ray emission spectrum of α-quartz taken from Ref. 5 (top).

shape of the upper valence band looks similar to that of O $2p$ PDOS. Figure 2 shows the calculated O $2p$ PDOS in comparison with the experimental O $K\alpha$ emission spectra for α-quartz by Takahashi, Okamoto, and Seo[33] measured by an electron-probe microanalyzer. Klein and Chun[34] reported similar spectra about two decades ago. These experimental spectra compare favorably with the calculated O $2p$ PDOS.

Si x-ray emission spectra provide information on how Si AO's contribute to chemical bonds in the valence bands. Figures 3 and 4 respectively show the Si K and L_{23} emission spectra calculated in the present study together with the experimental data by Wiech and Kurmaev.[5] As can be found through the comparison, all features of Si emission spectra from α-quartz are well reproduced by the calculation. From the examination of Si PDOS's, the influence of the inclusion of 4 more tetrahedra on the electronic structure of $(SiO_4)^{4-}$ cluster as well as the dependencies on Si-O-Si angle can be seen. However, differences in spectral shape are still small and these polymorphs are not easily distinguished only from the valence-band spectra.

IV. CONDUCTION-BAND SPECTRA

Figure 5 shows the sum of Si $3s$ PDOS and $3d$ PDOS obtained by the present calculation in comparison with experimental Si L_{23}-edge NEXAFS of α-quartz by Li *et al.*[19] Figure 6 displays the Si $3p$ PDOS together with Si K-edge NEXAFS of α-quartz. Similar to the cases of valence-band spectra, our PDOSs for α-quartz agree well with the NEXAFS at both edges. It means that the emission effects associated with the electronic transitions do not change the spectral shapes remarkably from those of PDOS at the ground state in these compounds. Assignments of all subband features can therefore be made without taking these effects into account explicitly.

MO levels obtained by the calculation of a simple $(SiO_4)^{4-}$ tetrahedron in the T_d symmetry is shown in Fig. 5. Although main features of NEXAFS can be assigned based on the MO levels of the $(SiO_4)^{4-}$ cluster calculation, experimental NEXAFS spectra look more complicated. Inclusion of neighboring tetrahedra is found to be essential in order to have good agreement of theoretical spectra with experimental ones in the energy range of ≤ 30 eV from the edge. The Si $3s$ orbital contributes to the $6a_1$ level in the $(SiO_4)^{4-}$ cluster as found in Fig. 5. In the $(Si_5O_{16})^{12-}$ clusters, the Si $3s$ unoccupied band exhibits two maxima due to non-nearest-neighbor interactions. These two peaks are denoted by A1 and A2 since they correspond to MO's in the a_1 symmetry block for a simple $(SiO_4)^{4-}$ tetrahedron in the T_d symmetry. The Si $3d$ orbital formed $6t_2$, $2e$, and $7t_2$ levels in the simple $(SiO_4)^{4-}$ tetrahedron. Each of these MO levels form 2 distinct subbands in the three $(Si_5O_{16})^{12-}$ clusters. They will be called T1 and T2 for $6t_2$, E1 and E2 for $2e$, and TT1 and TT2 for the $7t_2$ block, respectively. Tiny peaks can be found between T1 and T2 and E1 and E2 peaks in all of the theoretical curves in Fig. 5 and 6. They are denoted by T′ and E′, respectively, since they also originate from t_2 and e-block MO's in a tetrahedron cluster as will be discussed later.

The origin of the formation of these subbands is

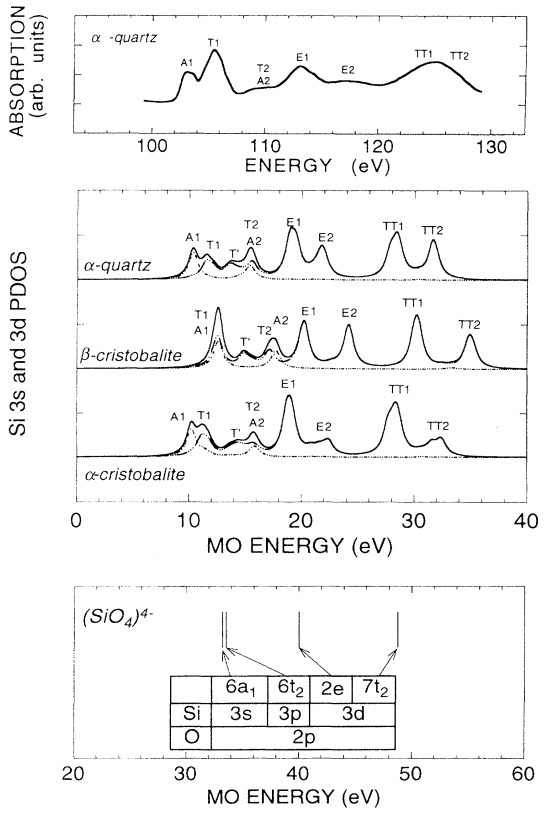

FIG. 5. Calculated Si $3s$ and $3d$ PDOS for three SiO_2 (middle) in comparison with experimental Si L_{23} x-ray-absorption spectrum of α-quartz taken from Ref. 19 (top) and MO levels of $(SiO_4)^{4-}$ together with their major components (bottom).

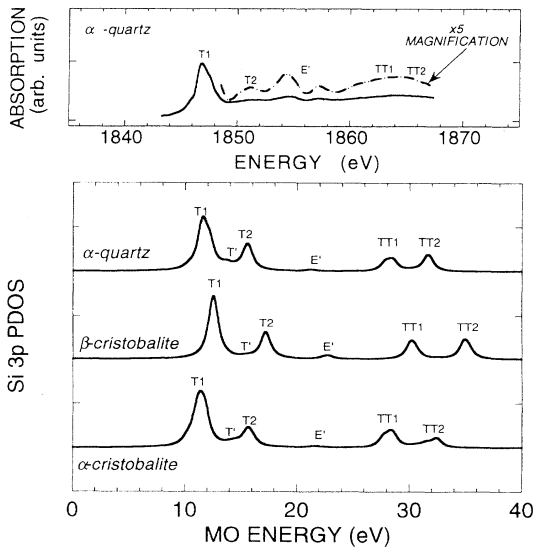

FIG. 6. Calculated Si $3p$ PDOS for three SiO_2 (bottom) in comparison with experimental Si K x-ray-absorption spectrum of α-quartz taken from Ref. 19 (top).

schematically drawn in Fig. 7. In the present calculation, a Si atom undergoing excitation is located at the center of the $(SiO_4)^{4-}$ tetrahedron, which is coordinated by four other tetrahedra. Bonding and antibonding interactions between MO's for each tetrahedral unit bring about the splitting of MO's. Results of Mulliken population analysis for the $(Si_5O_{16})^{12-}$ cluster taken from α-quartz are shown together in Fig. 7. The A1 level consists of the central Si AO's for 52%, and the 4 neighboring Si AO's for 32%. The rest of the AO fraction is due to oxygen atoms. This means that 52/32 = 1.6 times larger contribution to the A1 level is coming from the central Si atom compared with the neighboring four Si atoms. Similar calculation shows a 2.8 times larger contribution from the neighboring tetrahedra for the A2 level. The other three MO's in this block are mainly composed of Si AO's from the neighboring tetrahedra (86%), and the central tetrahedron makes a minor contribution (3%). As a result, these lines are weak but distinct. These peaks, which are mainly originated from AO's in the neighboring tetrahedra, correspond to the peaks shown by letters with a prime, i.e., A′, T′, E′, and TT′.

The influence of the $(SiO_4)^{4-}$ tetrahedron linkage is more clearly seen in the NEXAFS spectra than in the valence-band spectra, especially for the L_{23} edge shown in Fig. 5. The NEXAFS of β-cristobalite is different from those of α-quartz and α-cristobalite in two aspects. (1) The conduction-band edge energy is 2.14 and 2.04 eV greater in β-cristobalite than in α-cristobalite and α-quartz, respectively. On the other hand, the valence-band edge energy is 0.63 and 1.03 eV smaller also in β-cristobalite than in α-cristobalite and α-quartz, respectively. This implies that the band gap is greater in β-cristobalite than in the other two by 23% and 25% relative to the band gap of β-cristobalite. Although literature data on the precise band gap for three SiO_2 polymorphs are not available to the present authors' knowledge, it is in good agreement with the calculated band gap by Xu and Ching[13] using a first-principles orthogonalized linear combination of atomic orbitals band-structure calculation, which shows 16% and 18% greater band gap in β-cristobalite than α-cristobalite and α-quartz, respectively. (2) The energy difference between A1 and T1 peaks is 1.42 and 1.20 eV for α-quartz and α-cristobalite, respectively. On the other hand, the difference is only −0.07 eV for β-cristobalite. The separation between A1 and T1 in β-cristobalite is difficult to detect through experiments. As a result, β-cristobalite can be easily distinguished from other two polymorphs using the A1-T1 difference in spectral features of the Si L_{23} NEXAFS.

Unoccupied O 2p PDOS for three polymorphs are shown in Fig. 8 together with the experimental spectrum by Marcelli *et al.*[20] for α-quartz. Compared with the Si NEXAFS spectra, experimental energy resolution does not seem to be sufficiently high in the O K-edge NEXAFS. Recent investigation of the O K-edge NEXAFS of glassy SiO_2 found a similar spectrum with the same order of energy resolution.[21] However, comparison with the present theoretical spectrum makes it possible to assign two major peaks to A2+T2 and TT2. It also indicates that the strongest wide line centered at 538 eV is composed of several subbands: They are A1, T1, and T′ at the low-energy side and E1 and E2 at the high-energy side. Although definite conclusions require more accurate experimental spectra, the O K-edge NEXAFS seems to be less sensitive to the difference of the manner of $(SiO_4)^{4-}$ tetrahedral linkage than that of the Si L_{23}-edge NEXAFS.

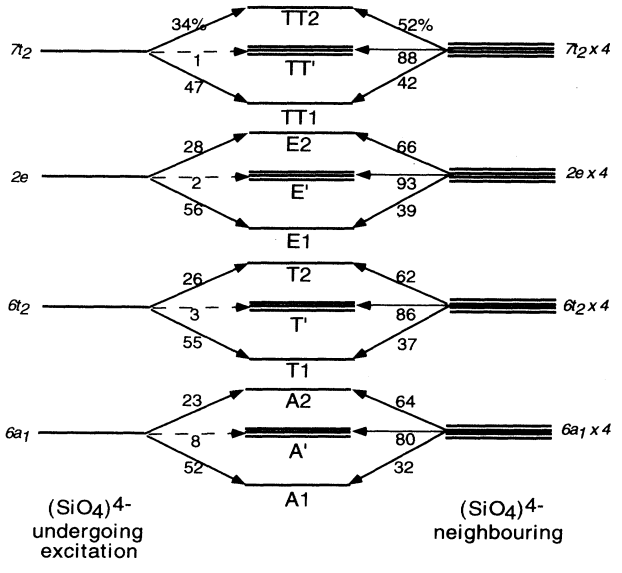

FIG. 7. Schematic of the formation of conduction-band structures in 4:2 coordinated SiO_2 as a result of hybridization of AO's originated from different tetrahedral units. Mulliken populations for Si atoms in different tetrahedral units at each of MO obtained for the α-quartz cluster are inserted.

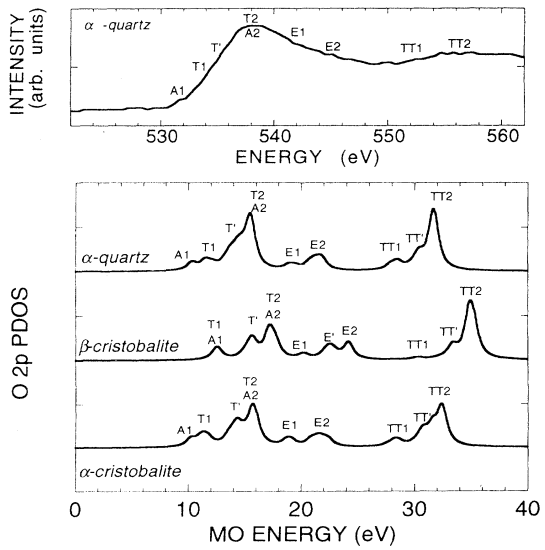

FIG. 8. Calculated O 2p PDOS for three SiO_2 (bottom) in comparison with experimental O K x-ray-absorption spectrum of α-quartz taken from Ref. 20 (top).

TABLE I. Calculated transition energies in comparison with experimental values. HOMO and LUMO denote highest occupied and lowest unoccupied molecular orbitals, respectively.

Transition	Experiment (eV)	Calculation (eV)	Difference
O 1*s* to HOMO	527	533	+1.2%
Si 1*s* to HOMO	1836	1835	−0.1%
Si 2*p* to HOMO	98	100	+2.1%
O 1*s* to LUMO	538	537	+0.8%
Si 1*s* to LUMO	1846	1836	−0.5%
Si 2*p* to LUMO	103	106	+3.1%

V. ABSOLUTE TRANSITION ENERGY

Absolute transition energies were calculated using the transition state method by Slater.[30] Table I shows the obtained results for 6 kinds of transitions in comparison with experimental values for α-quartz.[5,19,20,33] Spin polarization during the transition process was taken into account. For the x-ray-absorption process, transition energy, for example, from Si 1*s* to LUMO was obtained simply as $[\varepsilon(\text{LUMO}) - \varepsilon(\text{Si-}1s)]^T$ where ε is the one-electron MO energy for the transition state configuration, i.e., $(\text{Si-}1s)^{1.5}(\text{LUMO})^{0.5}$ as denoted by T. For the x-ray emission process, the transition state configuration, in which a half electron was removed from the core orbital undergoing excitation, was considered. The number of electrons in the cluster was reduced for 0.5 for the emission process. As can be seen, agreements between experimental and calculated values are within the error of 4%.

VI. SUMMARY

The DV-$X\alpha$ calculations on three clusters $(Si_5O_{16})^{12-}$, which are models for α-quartz, α-cristobalite, and β-cristobalite, have been conducted. The Si K, L_{23}, and O K XES and NEXAFS are compared with the calculated PDOS following the electric dipole selection rule. We find that our PDOS for α-quartz at the ground states agrees well with fine structures of the experimental NEXAFS in the range of ≤ 30 eV as well as the XES. This clearly shows that the emission effects associated with the electronic transitions do not change the spectral shapes remarkably from those of the PDOS in these compounds. Assignments of all subband features can therefore be made without taking these effects into account explicitly. As already pointed out about two decades ago, major features of valence-band structure of 4:2 coordinated SiO_2 can be explained by a simple calculation using the $(SiO_4)^{4-}$ tetrahedral unit. On the other hand, inclusion of neighboring tetrahedra is found to be essential in order to have good agreement of theoretical spectra with experimental ones for the conduction-band structure of SiO_2. Assignments of all subband features are made by taking into account the hybridization of AO's originated from different tetrahedral units. Conduction band ≤ 30 eV from the edge can be decomposed into 12 subbands, which are generated by bonding, antibonding, and nonbonding interaction of a_1, e, and two kinds of t_2 MO's in an individual $(SiO_4)^{4-}$ tetrahedron under the T_d symmetry. According to the present calculation, the difference in the manner of the $(SiO_4)^{4-}$ linkage as found in crystalline SiO_2 polymorphs can be most clearly seen in the Si L_{23}-edge NEXAFS.

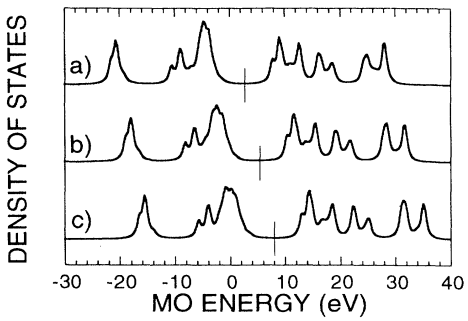

FIG. 9. Calculated DOS for α-quartz using three different sets of R_0 and V_0 given in Eq. (2). (a) $R_0 = 1.85$ Å and $V_0 = -40.8$ eV. (b) $R_0 = 1.43$ Å and $V_0 = -49.0$ eV. (c) $R_0 = 1.32$ Å and $V_0 = -68.0$ eV. Vertical short lines indicate the average energy of the highest occupied and the lowest unoccupied molecular orbitals.

Since the present calculation method requires neither periodic boundary conditions nor symmetry in clusters, it can readily extend to more complicated systems such as intergranular SiO_2 glassy phase in nonoxide ceramics and surface problems.

Note added in proof. The atomic coordinates that we have used for β-cristobalite are taken from an old literature data which shows the $O_h^7(Fd3m)$ structure. However, we noticed that the atoms are somewhat removed from these highly symmetrical positions in real β-cristobalite crystal. This is not included in the present calculation.

ACKNOWLEDGMENT

This work was supported by Grant-in-Aid for General Scientific Research from Ministry of Education Science and Culture of Japan under Contract No. 06650801.

APPENDIX

In order to know the uncertainty of the calculated results associated with the choice of the well potential for the basis-set generation, dependence on the parameters given in Eq. (2) is studied. Figure 9 compares the DOS of α-quartz obtained for three different sets of R_0 and V_0 in the present study using a $(Si_5O_{16})^{12-}$ cluster. The DOS shape is found to be not significantly altered by the choice of these values except for a small shift in the absolute MO energies as much as ± 3 eV in these cases. However, all MO energies including core levels are translated by almost the same amount: As a result, the transition energies calculated from these three examples are found

to be much less dependent on these parameters. For example, the transition energies of the first peak of Si L_{23}-edge XANES, which corresponds to the Si $2p$ to Al transition in our notation, were (a) 106.6 eV, (b) 106.2 eV and (c) 105.9 eV for three cases used in Fig. 9. The relative scattering of the transition energy is therefore $\pm 0.3\%$. Based on these results, we can conclude that the choice of these parameters affects the final results for a negligible amount at least in these compounds if they are chosen from the appropriate ranges.

[1]T. H. DiStefano and D. E. Eastman, Phys. Rev. Lett. **27**, 1560 (1971).

[2]B. Fischer, R. A. Pollak, T. H. DiStefano, and W. D. Grobman, Phys. Rev. B **15**, 3193 (1977).

[3]D. A. Stephenson and N. J. Binkowski, J. Non Cryst. Solids **22**, 399 (1976).

[4]G. Wiech, Solid State Commun. **52**, 803 (1984).

[5]G. Wiech and E. Z. Kurmaev, J. Phys. C **18**, 4393 (1985).

[6]J. A. Tossell, D. J. Vaughan, and K. H. Johnson, Chem. Phys. Lett. **20**, 329 (1973).

[7]S. T. Pantelides and W. A. Harrison, Phys. Rev. B **13**, 2667 (1976).

[8]R. B. Laughlin, J. D. Joannopoulos, and D. J. Chadi, Phys. Rev. B **20**, 5228 (1979).

[9]R. N. Nucho and A. Madhukar, Phys. Rev. B **21**, 1576 (1980).

[10]Y. P. Li and W. Y. Ching, Phys. Rev. B **31**, 2172 (1985).

[11]G. B. Cherlov, S. P. Friedman, E. Z. Kurmaev, G. Viech, and V. A. Gubanov, J. Non Cryst. Solids **94**, 276 (1987).

[12]A. Simunek, J. Vackar, and G. Wiech, J. Phys. Condens. Matter **5**, 867 (1993).

[13]Y. N. Xu and W. Y. Ching, Phys. Rev. B **44**, 11 048 (1991).

[14]G. A. D. Collins, D. W. J. Cruickshank, and A. Breeze, J. Chem. Soc. Faraday Trans. 2 **68**, 1189 (1972).

[15]F. C. Brown, R. Z. Bachrach, and M. Skibowski, Phys. Rev. B **15**, 4781 (1977).

[16]V. J. Nithianandam and S. E. Schnatterly, Phys. Rev. B **38**, 5547 (1988).

[17]Y. Baba. H. Yamamoto, and T. A. Sasaki, Phys. Rev. B **48**, 10 972 (1993).

[18]N. Nagashima, A. Nakano, K. Odata, M. Tamura, K. Sugawara, and K. Hayakawa, Phys. Rev. B **48**, 18 257 (1993).

[19]D. Li, G. M. Bancroft, M. Kasrai, M. E. Fleet, X. H. Feng, K. H. Tan, and B. X. Yang, Solid State Commun. **87**, 613 (1993).

[20]A. Marcelli, I. Davoli, A. Bianconi, J. Garcia, A. Gargano, C. R. Natoli, M. Benfatto, P. Chiaradia, M. Fantoni, E. Fritsch, G. Calas, and J. Petiau, J. Phys. (Paris) Colloq. **46**, C-8, 107 (1985).

[21]P. Lagarde, A. M. Flank, G. Tourillon, R. C. Liebermann, and J. P. Itie, J. Phys. (France) I **2**, 1043 (1992).

[22]T. Fujikawa, J. Phys. Soc. Jpn. **52**, 4001 (1983).

[23]D. G. J. Sutherland, M. Kasrai, G. M. Bancroft, Z. F. Liu, and K. H. Tan, Phys. Rev. B **48**, 14 989 (1993).

[24]X. Weng and P. Rez, Phys. Rev. B **39**, 7405 (1989).

[25]I. Tanaka, J. Kawai, and H. Adachi, Solid State Commun. **93**, 553 (1995).

[26]Y. Kowada, H. Adachi, M. Tatsumisago, and T. Minami, J. Non Cryst. Solids **150**, 318 (1992).

[27]J. Kawai, E. Uda, and M. Uda, in *Computer Aided Innovation of New Materials II*, edited by M. Doyama, J. Kihara, M. Tanaka, and R. Yamamoto (Elsevier, Amsterdam, 1993), p. 229.

[28]The DV method was first developed to solve the energy-band problems by D. E. Ellis and G. S. Painter, Phys. Rev. B **2**, 2887 (1970). This was first applied to the cluster calculation by F. W. Averill and D. E. Ellis, J. Chem. Phys. **59**, 6412 (1973). Self-consistent calculations were made by A. Rosén, D. E. Ellis, H. Adachi, and F. W. Averill, J. Chem. Phys. **65**, 3629 (1976). We use a modified version of this program which was described in detail in Ref. 29. In this version, the radial parts of the numerical basis functions can be optimized corresponding to the change of molecular charge density for each iteration.

[29]H. Adachi, M. Tsukada, and C. Satoko, J. Phys. Soc. Jpn. **45**, 875 (1978).

[30]J. C. Slater, *Quantum Theory of Molecules and Solids* (McGraw-Hill, New York, 1974), Vol. 4.

[31]R. G. Wyckoff, *Crystal Structures*, 2nd ed. (Interscience, New York, 1964).

[32]J. J. Yeh and I. Lindau, At. Data Nucl. Data Tables **32**, 1 (1985).

[33]H. Takahashi, T. Okamoto, and Y. Seo, J. Jpn. Inst. Met. **53**, 349 (1989).

[34]G. Klein and H. U. Chun, Phys. Status Solidi B **49**, 167 (1972).